Published in final edited form as:
Neuron. 2013 January 9; 77(1): 99–114. doi:10.1016/j.neuron.2012.10.033.

Mossy fiber-CA3 synapses mediate homeostatic plasticity in mature hippocampal neurons

Kea Joo Lee[*,1], **Bridget N. Queenan**[*,1,3], **Aaron M. Rozeboom**[1], **Ryan Bellmore**[1], **Seung T. Lim**[2,3], **Stefano Vicini**[1,2,3], and **Daniel T. S. Pak**[1,3,†]

[1]Department of Pharmacology & Physiology, Georgetown University Medical Center, Washington, DC 20057, USA.

[2]Department of Neuroscience, Georgetown University Medical Center, Washington, DC 20057, USA.

[3]Interdisciplinary Program in Neuroscience, Georgetown University Medical Center, Washington, DC 20057, USA.

SUMMARY

Network activity homeostatically alters synaptic efficacy to constrain neuronal output. However, it is unclear how such compensatory adaptations coexist with synaptic information storage, especially in established networks. Here, we report that in mature hippocampal neurons *in vitro*, network activity preferentially regulated excitatory synapses within the proximal dendrites of CA3 neurons. These homeostatic synapses exhibited morphological, functional, and molecular signatures of the specialized contacts between mossy fibers of dentate granule cells and thorny excrescences (TEs) of CA3 pyramidal neurons. *In vivo* TEs were also selectively and bidirectionally altered by chronic activity changes. TE formation required presynaptic synaptoporin and was suppressed by the activity-inducible kinase, Plk2. These results implicate the mossy fiber-TE synapse as an independently tunable gain control locus that permits efficacious homeostatic adjustment of mossy fiber-CA3 synapses, while preserving synaptic weights that may encode information elsewhere within the mature hippocampal circuit.

INTRODUCTION

Neuronal activity is capable of bidirectionally modifying the strength and size of excitatory synapses in the central nervous system, often by altering the postsynaptic accumulation of AMPA-type glutamate receptors (AMPARs) and dendritic spine morphology (Malinow and Malenka, 2002). Activity-dependent negative feedback mechanisms such as homeostatic synaptic plasticity (HSP) constrain the strength of excitatory transmission, promoting network stability (Turrigiano, 2008). However, it remains unclear how homeostatic synaptic adjustments are implemented without perturbing associative (Hebbian) plasticity-generated information potentially encoded as patterns of differential synaptic strength.

[†]Contact information: dtp6@georgetown.edu.
[*]These authors contributed equally to this work

In developing neurons, a form of HSP called synaptic scaling has been described in which a uniform, global multiplicative change occurs in all excitatory synapses (Turrigiano et al., 1998), thereby preserving relative synaptic weights (Turrigiano and Nelson, 2000). In older neurons, however, homeostatic changes at excitatory synapses do not seem to occur by multiplicative scaling (Burrone et al., 2002; Echegoyen et al., 2007; Goel and Lee, 2007; Thiagarajan et al., 2005; Wierenga et al., 2006). This developmental switch suggests the existence of an alternate, unidentified mechanism for the coexistence of homeostatic and associative plasticity in the adult brain.

Here, we found that homeostatic adaptation of excitatory synapses in mature hippocampal neurons occurred predominantly via regulation of thorny excrescences (TE), enigmatic dendritic spines whose functions have remained elusive a century after their initial description (Ramon y Cajal, 1911). *In vivo*, TEs are giant complexes of multiple spine heads with discrete active zones on a single neck, found mainly on proximal dendrites of hippocampal CA3 pyramidal cells apposed to equally large mossy fiber terminals of dentate gyrus (DG) granule cells (Amaral and Dent, 1981; Chicurel and Harris, 1992). TEs are highly plastic and morphologically responsive to diverse environmental inputs (Galimberti et al., 2006) including disease states (Kolomeets et al., 2007; Tsamis et al., 2010), stress and learning (Stewart et al., 2005), and hormonal stimuli (Hatanaka et al., 2009), but their physiological functions are poorly understood. We demonstrate that mossy fiber-TE synapses provide independently tunable excitatory gain control in dedicated CA3 proximal dendritic domains, thereby permitting homeostatic adjustment without perturbing synaptic information storage at other synaptic contacts within the hippocampal network.

RESULTS

Homeostatic adaptation at proximal but not distal synapses

To investigate mechanisms of HSP in established networks, we manipulated the activity state of mature (>21 days *in vitro* [DIV]) cultured hippocampal neurons. Chronic inactivity, induced with the reversible sodium channel blocker tetrodotoxin (TTX, 1 μM, 24 hr), increased both the amplitude and frequency of AMPAR-mediated miniature excitatory postsynaptic currents (mEPSCs) (nontreated (NT): 8.5±0.47 pA, 5.5±0.47 Hz; TTX: 12.1±0.92 pA, 9.3±0.87 Hz; $P<0.001$ vs. NT; one-way ANOVA and *post hoc* Tukey test), while chronic hyperactivity, induced by the $GABA_A$ receptor antagonist picrotoxin (PTX, 100 μM, 24 hr), decreased both mEPSC amplitude and frequency (PTX: 6.1±0.34 pA, 3.6±0.41 Hz; $P<0.01$ vs. NT) (Figure 1B–D). These results support previous reports of bidirectional compensatory changes in synaptic efficacy after network activity alterations (O'Brien et al., 1998; Pak and Sheng, 2003; Seeburg et al., 2008; Thiagarajan et al., 2005; Turrigiano et al., 1998).

To determine whether HSP occurred uniformly throughout the dendritic tree, we examined excitatory synapses via immunostaining against the scaffold protein Shank, a postsynaptic density (PSD) marker. Under basal conditions we observed a uniform distribution of Shank puncta along dendrites of pyramidal neurons (Figure 1A, F–G, see **Methods** for morphological identification). In parallel to the observed changes in mEPSCs, PTX provoked a loss of Shank while TTX markedly increased Shank levels (Figure 1A). Interestingly, these changes occurred exclusively within proximal dendrites (0–40 μm from soma), with no change observed distally (>40 μm) (Figure 1F–G) ($P<0.001$ vs. NT; one-way ANOVA and Tukey test). Similar results were found for other PSD proteins, including PSD-95 (Figure 1G), Homer, α-actinin and SPAR (data not shown). The vast majority of PSD-95/Shank puncta included in our analyses were apposed to presynaptic markers bassoon or synaptophysin in both proximal and distal dendrites, under basal and TTX-

treated conditions (Figures S1A–B, 4G, and S4G) and thus likely represented authentic synapses.

Miniature EPSCs originating at proximal synapses have faster kinetics than distal ones when recorded at the soma, due to distance-dependent dendritic filtering (Forti et al., 1997; Magee and Cook, 2000). Indeed, AMPAR-mEPSC rise times were significantly faster with TTX and slower with PTX (in msec: NT 4.4±0.19, TTX 3.5±0.16, PTX 4.9±0.15; $P<0.05$ vs. NT; one-way ANOVA and Tukey test) (Figure 1E), suggesting that the proportion of proximal synaptic events is increased with inactivity and diminished with overactivity.

Proximal PSD-95 upregulation was also observed with 24 hr activity blockade using antagonists of NMDARs (APV, 100 μM), AMPARs (CNQX, 40 μM), or L-type voltage-gated calcium channels (nimodipine, 5 μM) (TTX: 324.8±40.6% of NT, nim: 300.2±48.7%, APV: 237.8±18.5 %, all $P<0.001$ vs. NT; CNQX: 160.8±14.9%, $P>0.05$; one-way ANOVA and Tukey test) (Figure 1H–I). Under no conditions did we observe changes in distal synapses. Proximal adaptation was calcium-mediated, as elevating cytosolic Ca^{2+} via thapsigargin (1 μM)-mediated emptying of internal stores (Reyes and Stanton, 1996) abolished the proximal upregulation seen in all activity conditions tested (TTX+thaps: 75.4±9.0% of NT; nim+thaps: 35.5±5.9%; APV+thaps: 89.4±16.6%; CNQX+thaps: 52.0±9.0% of NT; all $P<0.05$ vs. no thaps; one-way ANOVA and Tukey test) (Figure 1H–I). Conversely, removal of extracellular Ca^{2+} with EGTA (1.5 mM) induced a time-dependent, reversible proximal upregulation (Figure S1C–D). TTX-induced proximal upregulation was also reversible after 48 hrs of washout (Figure S1C–D), indicating a lack of nonspecific toxicity.

Functional adaptation at proximal but not distal synapses

To directly test if HSP of excitatory synapses were confined to proximal dendrites in mature hippocampal neurons, we locally stimulated synaptic subpopulations by pressure-applying hyperosmolar sucrose (Bekkers and Stevens, 1996; Magee and Cook, 2000) to proximal (<30 μm) and distal (>100 μm) portions of dendrites from control and activity-manipulated pyramidal neurons (Figure 2A–B). Sucrose application successfully evoked synaptic currents at all locations (shown by a significant increase in mEPSC frequency over baseline) (Figure S2A–B), and, as expected, proximally evoked events were significantly faster than distal ones on the same dendrite (Figure S2D).

Following activity manipulation, we observed bidirectional changes in the frequency of events evoked proximally (Figure S2A) with no significant differences in distal event frequency (Figure S2B). We also observed bidirectional changes in the amplitude of proximally evoked mEPSCs (PTX 7.6±1.58 pA, NT 9.9±1.07 pA, TTX 14.1±1.75 pA; $P=0.026$, one-way ANOVA) with no corresponding changes in distal amplitude (PTX 6.3±1.06 pA, NT 8.1±0.74 pA, TTX 10.0±0.98 pA; $P=0.052$, one-way ANOVA) (Figure 2C, S2C). Distal stimulation elicited currents of similar “synaptic weight” (evoked vs. baseline amplitude) in all activity conditions (NT 11.2±4.4% increase over baseline; TTX 15.4±6.9%; PTX 5.7±6.0%; $P=0.58$, one-way ANOVA), suggesting that distal synaptic strength remained constant relative to the global synaptic population (Figure 2D). However, the relative amplitude of proximal synapses was much larger in TTX-treated neurons and smaller in PTX-treated neurons (NT 27.8±4.1% increase over baseline; TTX 60.0±13.5%; PTX 13.4±7.4%; $P=0.0093$, one-way ANOVA) (Figure 2D). Thus, proximal synaptic weight was preferentially altered by network activity.

The higher frequency and amplitude of TTX-treated neurons (Figure 1C–D) raised the possibility that the increased proximal amplitude observed with local stimulation may be due to the collision of monoquantal events or to contamination of the evoked population by

events originating elsewhere in the dendritic tree. We therefore bath applied the nonselective glutamatergic antagonist kynurenic acid (KynA, 200 μM) to globally diminish mEPSC amplitude and therefore detected frequency (Mellor and Nicoll, 2001). The low-affinity binding of KynA allowed the blockade to be rapidly and locally displaced by sucrose application (Figure 2E). During KynA blockade, baseline mEPSC amplitude and frequency did not differ significantly between control and TTX-treated neurons (NT 7.7±0.68 pA, 3.9±0.99 Hz; TTX 8.7±0.46 pA, 3.0±0.93 Hz; $P>0.21$), and mEPSC frequency was comparable after proximal stimulation (NT 13.4±1.55 Hz; TTX 12.5±4.17 Hz; $P=0.828$). However, we again observed a large increase in the amplitude of proximally evoked mEPSCs (NT 6.9±0.34 pA,; TTX 10.1±1.53 pA; $P=0.027$, one-way ANOVA and Tukey test) with no change in distal amplitude (NT: 6.4±0.40 pA; TTX 7.3±0.31 pA; $P>0.05$) (Figure 2F). Together with the morphological data, these results indicate that proximal synapses are selectively altered by activity.

Consistent with previous reports (O'Brien et al., 1998; Wierenga et al., 2005), chronic inactivity induced robust increases in surface and total levels of both GluA1 (Figure 2G–H) and GluA2 (Figure 2I) AMPAR subunits. However, these increases were observed only at proximal synapses (surface GluA1: NT 1.0±0.06, TTX 2.6±0.19; total GluA1: NT 1.0±0.24, TTX 2.0±0.25; surface GluA2: NT 1.0±0.17, TTX 1.7±0.30; total GluA2: NT 1.0±0.11, TTX 1.5±0.12; $P<0.05$, t-test vs. NT), with no changes observed in distal dendrites (surface GluA1: NT 1.00±0.09, TTX 1.05±0.08; total GluA1: NT 1.00±0.25, TTX 1.06±0.15; surface GluA2: NT 1.00±0.16, TTX 0.94±0.19; total GluA2: NT 1.00±0.14, TTX 1.17±0.13; $P>0.38$, t-test vs. NT) (Figure 2G–I). The increase was more pronounced for GluA1 than GluA2, and indeed homomeric GluA1 AMPARs have been reported to mediate homeostatic adaptation in response to certain inactivity paradigms (Thiagarajan et al., 2005). However, philanthotoxin-433 (PhlTx, 1 μM), which blocks AMPARs lacking the GluA2 subunit, did not revert the increased amplitude or faster rise time in TTX-treated neurons to control levels, but in fact increased mEPSC amplitude further (TTX+PhlTx: 106.8±2.7% of TTX; $P=0.02$, paired t-test) (Figure S2E–G). Unlike AMPARs, levels of the obligatory GluN1 subunit of NMDARs were not increased in TTX-treated proximal dendrites (Figure S2H–J). Homeostatic strengthening in mature neurons therefore appears to occur via preferential insertion of GluA1/2 heteromeric AMPARs into proximal synapses.

Homeostatic adaptation to inactivity occurs preferentially in CA3 neurons

In our initial studies, we found that ~70% of morphologically identified pyramidal neurons responded homeostatically, as assayed by either immunocytochemistry or electrophysiology. To determine whether HSP occurred only in a subset of excitatory cell types, we used established immunocytochemical markers to distinguish among the three major excitatory cell types of the hippocampus, namely CA1/CA3 pyramidal neurons and DG granule cells. Immunostaining for CTIP2, a transcription factor expressed in CA1 and DG but not CA3 neurons (Williams et al., 2011) (Figure S3A), revealed that most CTIP2-negative (putative CA3) neurons displayed robust proximal synaptic upregulation in response to TTX (NT 2.2±1.5%; TTX 78.3±4.2%), while proximal immunoreactivity was not altered in CTIP2-positive (DG/CA1) neurons (NT 1.0±2.01%; TTX 3.8±3.8%; $P=0.25$, t-test vs. NT) (Figure 3A–B).

To confirm that HSP was CA3-specific, we used Py antibody to positively label CA3 neurons (Woodhams et al., 1989; Williams et al., 2011). Under basal conditions, few CA3 cells displayed proximal upregulation (Figure 3C). PTX treatment further decreased this percentage, while TTX caused the great majority of CA3 cells to develop proximal dendritic PSD-95 clusters (NT 14±4%; TTX 91±2.8%; PTX 4±1.6%; $P<0.05$, t-test vs. NT) (Figure 3C–D). Total Shank immunoreactivity was bidirectionally modulated in proximal, not distal, dendrites of Py^+ CA3 neurons (proximal: NT 1.0±0.12, TTX 4.9±0.82, PTX 0.3±0.04;

P<0.001; distal: NT 0.8±0.10, TTX 1.1±0.17, PTX 0.9±0.08; *P*>0.27; t-test vs. NT) (Figure 3E).

Within the CTIP2+ subpopulation, DG cells were readily distinguished by having smaller somata and fewer primary dendrites than CA1 cells (Figure S3A–D). We confirmed that these morphologically identified DG cells were immunopositive for the DG-specific transcription factor Prox1 (Williams et al., 2011) and were unresponsive to TTX treatment (Figure S3E). CA3 cells had 5–7 primary neurites which were thicker and branched closer to the soma than CA1 cells which had more and thinner primary neurites (Figure S3A–D and data not shown). We therefore used these morphological criteria to record cell type-specific functional responses in GFP-transfected neurons.

Importantly, CA3 neurons exhibited increased mEPSC amplitude and frequency with TTX (NT: 9.0±1.2 pA, 5.7±1.4 Hz; TTX: 13.2±1.0 pA, 19.2±2.9 Hz, *P*<0.05, t-test vs. NT), whereas neither parameter was significantly altered in DG or CA1 neurons (DG: NT, 10.2±0.53 pA, 8.5±1.3 Hz; TTX, 9.0±0.94 pA, 10.1±2.4 Hz; CA1: NT, 12.5±1.4 pA, 4.8±2.1 Hz; TTX, 12.3±1.9 pA, 9.9±3.5 Hz; *P*>0.26 vs. NT) (Figure 3F–H). Collectively, these findings suggest that homeostatic adaptation of mature hippocampal neurons occurs preferentially in the proximal dendrites of CA3 neurons.

Chronic inactivity generates giant multi-synaptic proximal spines

The proximal dendrites of CA3 neurons *in vivo* are the site of “thorny excrescences,” large, specialized dendritic spines containing multiple postsynaptic sites. We therefore examined whether proximal CA3 homeostatic adaptation proceeded via formation of *in vitro* thorny excrescences. We visualized spine morphology by infecting neurons with Sindbis virus expressing enhanced green fluorescent protein (GFP) as a neuronal fill (Figure 4A–C). TTX induced a pronounced increase of proximal spine head size (NT 0.30±0.01 μm^2; TTX 0.50±0.04, *P*<0.001, t-test vs. NT), with no change in distal spine head area (NT 0.25±0.01 μm^2, TTX 0.24±0.01; *P*=0.7 vs. NT) (Figure 4A–B). This effect was due to selective enlargement of the largest spine population rather than uniform global expansion (Figure 4C). Remarkably, the largest spine sizes attained in TTX were ~10 times the mean head area and ~50 times the mean volume of control spines (Figure S4A). TTX did not alter spine or filopodia density or spine length, however (Figure S4B–D), suggesting that chronic inactivity does not influence general spine formation or maintenance.

We investigated whether these giant proximal spines contained expanded synapses, as previously observed following inactivity (Carpenter-Hyland and Chandler, 2006; Murthy et al., 2001; Thiagarajan et al., 2005). Co-staining for PSD-95 and GFP fill (Figure 4A) showed that spine head size was strongly correlated with total PSD-95 immunoreactivity under all conditions tested (Figure S4E). Surprisingly, we observed at higher magnification that the enlarged proximal spines formed with TTX frequently contained not simply larger synapses, but clusters of normal-sized synapses (Figure 4A, D). Such “cluster synapses”, appearing exclusively on proximal dendrites, formed within 4 hr in TTX (Figure 4E–F), after which cluster number quickly rose and plateaued by 24 hr (Figure S4F), attaining an average of ~64 (and maximum of ~130) clusters per cell at 72 hr (Figure 4E). The number of PSD-95 puncta per cluster increased linearly as a function of time, with a mean of ~8 (and upper limit of ~40) PSDs per spine at 72 hr (Figure S4F). Thus, we observed a time-dependent linear increase in total proximal synapses correlated with the number of giant clusters formed (Figure 4E–F).

To determine whether these multi-PSD clusters represented bona fide synapses, we co-stained for Shank and the presynaptic marker synaptophysin (Syn). Syn and Shank intensities strongly correlated at all times (Figures 4G and S4G), and Syn staining was

accordingly increased only within proximal dendrites following TTX treatment (Figure 4H). Enlarged Shank clusters were precisely apposed to presynaptic sites of commensurate size and complexity; these large Syn clusters were typically comprised of individually discernible subpuncta paired with discrete PSDs (Figure 4H). Additional presynaptic markers bassoon and vGlut1 yielded similar results (data not shown). No change in the number of presynaptic sites was observed when Syn clusters were scored as a single bouton (Figure 4H), indicating that existing presynaptic terminals likely became elaborated with inactivity, as previously suggested (Thiagarajan et al., 2005). These results demonstrate that pre- and postsynaptic specializations are coordinately expanded to form clustered synapses upon giant proximal spines in response to inactivity.

In contrast to mature neurons, TTX treatment of immature CA3 neurons (12 DIV) induced a uniform upregulation of PSD-95 along dendrites (Figure S4H–K), suggestive of synaptic scaling. These results suggest a developmental switch from global synaptic scaling in young neurons to spatially segregated HSP in mature proximal dendrites.

Proximal clusters display properties of mossy fiber-CA3 synapses

In vivo, CA3 TEs are innervated by the large, complex mossy fiber (MF) terminals of DG cells. MF boutons preferentially contact CA3 cells *in vitro* as well (Williams et al., 2011). MF-TE synapses in brain are specifically enriched in puncta adherentia junctions comprised of cadherin-catenin and nectin-afadin cell adhesion systems (Takai, 2003). We therefore examined whether the TTX-induced *in vitro* clusters contained l-afadin, an actin-associated scaffold and intracellular adapter for nectin adhesion molecules. Under basal conditions, we observed weak lafadin immunoreactivity at excitatory synapses (Figure 5A). Chronic inactivity markedly upregulated l-afadin only in proximal synapses (Figure 5A–B) (proximal: NT 1.0±0.31, TTX 3.3±0.50, $P<0.001$; distal: NT 0.25±0.08, TTX 0.40±0.10, $P=0.25$; t-test vs. NT), particularly at giant cluster synapses in which multiple l-afadin and PSD-95 puncta were clearly interdigitated (Figure 5A, inset).

Mossy fiber boutons are also selectively marked by the presynaptic vesicle-associated protein synaptoporin (SPO; also called synaptophysin 2) (Singec et al., 2002). We found that TTX markedly increased SPO immunoreactivity along proximal but not distal dendrites (Figure 5C–D) (proximal: NT 1.0±0.37, TTX 4.0±1.2, $P<0.05$; distal: NT 0.34±0.12, TTX 0.62±0.19, $P=0.24$). The TTX-induced proximal cluster synapses labeled with PSD-95 were apposed to particularly large puncta immunoreactive for SPO (Figure 5C, insets), indicating that inactivity promotes presynaptic MF elaboration opposite proximal TE expansion in CA3 cells.

We hypothesized that the increase in AMPAR-mEPSC frequency after TTX treatment was due to selective upregulation of MF-CA3 synapses. We therefore performed a synaptotagmin uptake assay to determine presynaptic release at SPO-positive terminals. While TTX treatment again increased proximal SPO levels (Figure S5A–B), inactivity did not significantly increase either proximal or distal synaptotagmin levels (TTX proximal: 131.7±17.9% of NT proximal; TTX distal: 41.8±4.8% of NT distal; Figure S5A,C). However, TTX treatment caused a massive redistribution of synaptotagmin to SPO-positive boutons (NT proximal: 31.8±5.3% synaptotagmin colocalization with SPO, TTX proximal: 80.9±3.7%; NT distal: 16.6±4.4%, TTX distal: 52.0±8.7%; $P<0.01$; Figure S5A,D), suggesting that inactivity reallocates presynaptic efficacy towards MF-CA3 synapses as has been observed in organotypic slice culture (Kim and Tsien, 2008; Mitra et al., 2012).

Hippocampal MF synapses are the most powerful hippocampal synapses known (Henze et al., 1997; Jonas et al., 1993), making it possible that the inactivity-induced increase in AMPAR-mEPSC amplitude was due to selective increases in presynaptic release from these

terminals. We therefore quantified the number of large amplitude mEPSCs (>95th percentile amplitude value for control neurons, 20 pA) recorded before and after mGluR2 activation, which is known to block MF transmission in acute slice (Mellor and Nicoll, 2001). Using the synaptotagmin uptake assay to validate the *in vitro* MF blockade, we found that acute mGluR2 agonist application decreased the colocalization of synaptotagmin with SPO in both proximal and distal dendrites (Figure S5D). Acute MF blockade with mGluR2 agonists LY487379 (5 μM) or DCGIV (10 μM, data not shown) significantly decreased the number of large amplitude mEPSCs observed in TTX-treated neurons (events/minute: baseline, 58.2±21.8; LY487379, 23.5±11.8, P=0.032, paired t-test vs. baseline), without altering the number of small amplitude events (<20 pA) (Figure 5E–F, S5E). MF blockade also abolished the significant differences in mEPSC amplitude observed with homeostatic adaptation (in pA, baseline: NT 8.5±0.92, TTX 11.5±1.0, PTX 6.1±0.52; P<0.01, one-way ANOVA; LY487379: NT 8.1±0.86, TTX 10.0±0.67, PTX 6.9±1.2; P=0.08) (Figure 5G), suggesting that changes in MF transmission largely account for the observed homeostatic changes in amplitude.

Presynaptic upregulation of synaptoporin is required for HSP

To confirm that SPO-positive MF terminals innervate CA3 neurons *in vitro*, we immunostained GFP-transfected neurons with PSD-95 and the CA3-specific marker, Py. SPO-positive boutons from GFP-transfected DG neurons preferentially targeted Py-positive CA3 cells (~80 %; Figure S6A–B), reflecting a high specificity of DG-CA3 synaptic connections in culture.

To test the requirement of MF upregulation for inactivity-induced TE formation, we used RNA interference (RNAi)-mediated knockdown of SPO (validated in Figure S6C–E). Neurons were transfected with control vector (pLL3.7), SPO-shRNA, or SPO-shRNA with an RNAi-insensitive SPO rescue construct for 2 days before 24 hr of TTX treatment. MF axonal processes from GFP-expressing DG neurons were traced to identify the postsynaptic contacts of SPO-positive terminals (Figure 6A, Figure S6A–B, F). Following TTX treatment, MF boutons (circles in Figure 6A) contacted the large PSD-95 immunoreactive puncta in proximal CA3 dendrites. SPO knockdown in presynaptic MF terminals abolished TTX-mediated enlargement of apposed PSD-95 puncta, while coexpression of SPO-shRNA and SPO rescue constructs restored the TTX-induced increase in PSD-95 puncta intensity in proximal CA3 synapses (Figure 6A–C) (pLL3.7 1.0±0.11; pLL3.7+TTX 1.8±0.28; SPO shRNA 0.4±0.06; SPO shRNA+TTX 0.6±0.08; SPO shRNA+rescue 1.8±0.22; SPO shRNA +rescue+TTX 2.4±0.34; P<0.05, one-way ANOVA and Tukey test). SPO knockdown and rescue had no effect on MF bouton size, however (Figure 6C) (pLL3.7 1.1±0.09 μm^2; pLL3.7+TTX 1.2±0.08; SPO shRNA 1.2±0.13; SPO shRNA+TTX 1.1±0.08; SPO shRNA +rescue 1.0±0.09; SPO shRNA+rescue+TTX 0.9±0.09; P>0.15, one-way ANOVA). Together, these findings suggest that Spo function is required for inactivity-induced upregulation of presynaptic MF function and subsequent expansion of postsynaptic TE, but not for structural enlargement of MF terminals.

We next examined the functional consequences of SPO knockdown and rescue by recording AMPAR-mEPSCs from the postsynaptic targets of GFP-expressing DG neurons. TTX treatment induced a significant increase in both mEPSC amplitude and frequency in DG targets (Figure 6D–F) (pLL3.7: 17.2±0.34 pA, 9.5±1.6 Hz; pLL3.7+TTX: 23.0±1.4 pA, 19.9±1.8 Hz; P<0.01 vs. pLL3.7, one-way ANOVA and Tukey test). SPO knockdown in presynaptic DG cells prevented the TTX-induced increase in both mEPSC amplitude and frequency (SPO shRNA: 16.3±0.4 pA, 9.6±0.8 Hz; SPO shRNA+TTX: 16.9±0.4 pA, 12.0±1.3 Hz, P>0.05 vs. pLL3.7, ++ P<0.01 vs. pLL3.7+TTX), while SPO rescue was sufficient to elevate mEPSC amplitude and frequency to TTX levels (Figure 6D–F) (SPO shRNA+rescue: 22.1±0.6 pA, 17.8±1.9 Hz; SPO shRNA+rescue+TTX: 21.1±1.7 pA,

23.2±3.4 Hz; $P<0.05$ vs. pLL3.7, $P>0.05$ vs. pLL3.7+TTX). Taken together, these results indicate that presynaptic SPO is necessary and sufficient for the homeostatic upregulation of mossy fiber-CA3 synapses.

Physiological regulation of thorny excrescences in vivo

To test whether activity also regulates TEs *in vivo*, we altered neuronal activity in 3-month-old wild-type (WT) mice via chronic pharmacological manipulation of network inhibition. Activity was globally enhanced with the $GABA_A$ receptor antagonist PTX, delivered at sub-seizure threshold doses (1 mg/kg, i.p.), or dampened with the $GABA_A$ receptor positive allosteric modulator diazepam (Dzp, 2 mg/kg, i.p.). We confirmed that, similar to TTX, diazepam (Dzp, 1 μM, 24 hr) induced the formation of giant proximal synapses *in vitro* (Figure S7A–B). After 2 weeks of daily injection of Dzp, PTX, or vehicle control, we used Golgi staining to examine the effects of chronic network activity modulation on dendritic spine morphology in the adult mouse hippocampus (Figure 7A,E,G). We observed that network activity bidirectionally altered TE morphology in proximal dendrites of CA3 neurons (Figure 7A–B): total TE area was dramatically larger following chronic inactivity and smaller following chronic hyperactivity when compared to vehicle control-treated mice (NT 19.8±1.4 μm^2, Dzp 30.9±3.5, PTX 12.6±2.1; $P<0.05$, t-test vs. NT). Chronic inactivity significantly increased the size of individual TEs (NT 4.1±0.33 μm^2, Dzp 6.4±0.72, PTX 3.9±0.65; $P<0.05$) (Figure 7C), while chronic hyperactivity significantly decreased the number of proximal TEs (NT 4.8±0.20 TE, Dzp 4.8±0.49, PTX 3.6±0.32; $P<0.05$) (Figure 7D), likely because individual TE size shrank below the morphological criterion for scoring protrusions as TEs rather than spines (see **Methods**).

To determine whether network activity specifically regulates TE morphology, we examined dendritic spines in the distal apical dendrites of CA3 (Figure 7E–F) and CA1 (Figure 7G–H) pyramidal neurons. We observed no significant differences in spine density (Figure 7F,H) (CA3: NT 10.1±0.40 spines/10μm, Dzp 10.8±0.41, PTX 10.1±0.50; $P=0.46$; CA1: NT 6.8±0.19, Dzp 7.2±0.34, PTX 6.9±0.29; $P=0.58$; one-way ANOVA), spine head area (Figure S7C,E) or spine length (Figure S7D,F) in distal CA3 or CA1 dendrites. The proximal apical dendrites of CA1 neurons are normally devoid of spines and we observed no increases in spine density with Dzp (data not shown). These results suggest that global network activity bidirectionally and preferentially alters TE morphology and structural plasticity in the adult hippocampus.

To examine the mechanisms of proximal homeostatic TE regulation, we investigated the role of Plk2, an activity-inducible kinase which displays a striking high-proximal to low-distal gradient of expression upon induction (Pak and Sheng, 2003) and is known to mediate homeostatic spine and synapse loss (Lee et al., 2011; Pak and Sheng, 2003). *In vitro*, overexpression of Plk2 induced downregulation of proximal but not distal synapses under basal conditions (Pak and Sheng, 2003) and blocked giant cluster synapse formation in TTX-treated cultured neurons (Figure S7G–H). Conversely, overexpression of a dominant-negative kinase-dead Plk2 mutant (DN-Plk2) induced significant increases in proximal, but not distal, Shank immunoreactivity under basal conditions (Figure S7G–H). These results suggest that Plk2 mediates the selective homeostatic adaptation of proximal synapses in mature hippocampal neurons, by negatively constraining proximal TE expansion.

We therefore analyzed TE morphology in previously generated transgenic mice with forebrain-specific expression of DN-Plk2 (Lee et al., 2011). Golgi analysis revealed that CA3 TE area was massively enlarged in 3-month-old DN-Plk2 transgenic mice compared to WT littermates (WT 18.9±2.9 μm^2, DN-Plk2 33.2±4.0, $P<0.05$, t-test vs WT) (Figure 7I–J). Similar to the TE overgrowth induced by diazepam, we observed significant increases in individual TE area in DN-Plk2 transgenic animals (WT 5.1±0.41 μm^2, DN-Plk2 7.0±0.18,

P<0.01) (Figure 7K), with no change in proximal TE number (WT 3.8±0.52, DN-Plk2 4.5±0.42, *P*=0.32) (Figure 7L). Activity-dependent expression of Plk2 within proximal dendrites may thus link synaptic activity level to homeostatic regulation of TE *in vivo*.

DISCUSSION

We demonstrated that in mature hippocampal neurons, HSP of excitatory synapses is not globally distributed but highly localized, occurring predominantly at proximal synapses between CA3 and DG neurons. This functional division of homeostatic adaptation underscores the importance of differentiating cell type for *in vitro* studies. Chronic inactivity generated *in vitro* TEs, which paralleled *in vivo* excrescences with respect to morphology, number and size; preand postsynaptic molecular composition; cell-type specificity; and functional synaptic properties. Moreover, activity modulation bidirectionally induced similar compensatory structural plasticity in hippocampal CA3 TEs *in vivo*. The robust expansion of TEs in response to a variety of inactivity regimes suggests TE are designated homeostatic gain control structures that boost excitatory drive in the mature hippocampus.

Dendritic subcompartmentalization of plasticity

Our results shed light on the observation that neurons undergo a developmental switch from synaptic scaling in young neurons to nonmultiplicative HSP in mature preparations (Figure 8A). In relatively young neurons (DIV11), CA3 neurons express a global scaling of excitatory synapse size in response to TTX. Following the bulk of synaptogenesis (>21 DIV), CA3 neurons lose the ability to undergo scaling, and proximal synapses appear to assume responsibility as a primary locus of homeostatic plasticity. This conclusion is supported by morphological analysis of excitatory synapses and dendritic spines, as well as by direct local stimulation of proximal and distal dendrites. Chronic inactivity produced fast and exceptionally large amplitude AMPAR-mEPSCs that are unlikely to originate in distal dendrites, due to distance-dependent attenuation of current amplitude and kinetics (Forti et al., 1997; Magee and Cook, 2000). These larger, faster currents cannot be explained by a subunit switch to higher conductance, faster GluA1 homomeric AMPARs (Thiagarajan et al., 2005), as philanthotoxin-433 blockade of GluA2-lacking receptors did not return mEPSC amplitude or rise times to control levels. Collectively, these multiple independent approaches argue that proximal excitatory synapses are the principal targets of regulation with chronic activity modulation.

The existence of potent HSP mechanisms in proximal dendrites does not exclude a role for distal synapses in HSP of mature neurons. Indeed, mEPSC frequency seems to be more globally downregulated in PTX, consistent with previous studies showing that the activity-inducible homeostatic negative regulator Plk2 is capable of mediating neuron-wide reductions in surface GluA2 levels (Evers et al., 2010), in addition to negatively regulating proximal dendritic TEs. This global phenomenon with chronic overactivity may reflect the more limited dynamic range for homeostatic downregulation of proximal synapses compared to their remarkable potential for expansion. Since hyperactivity poses an excitotoxic threat, it is likely that multiple homeostatic adaptations work in series or parallel (Pozo and Goda, 2010). It is also possible that regulation of distal dendritic synapses could be marshaled as a secondary layer of HSP control on a slower timescale, for example in the face of extremely prolonged periods of inactivity that cannot be surmounted by proximal mechanisms alone.

Excrescences as homeostatic gain control synapses

We envision that the compartmentalization of HSP to the proximal dendrites of CA3 neurons offers several advantages, being logistically efficient and bioenergetically

conservative. TEs have a theoretical cell-wide dynamic range of several thousand TE synapses per CA3 neuron, efficaciously situated near the soma and axon hillock where incoming dendritic signals are integrated into a firing decision. TEs may powerfully modulate neuronal excitability by selectively altering the number and strength of the strongest synaptic population, as assessed by AMPAR abundance and mEPSCs amplitude, PSD and dendritic spine size, presynaptic terminal strength, and synaptic location.

TE enlargement occurred without change in the number of boutons or dendritic spines, suggesting modulation of preexisting synapses with inactivity. However, as TE synapses exhibit divided pre- and postsynaptic clusters, it is likely that homeostatic regulation in older CA3 neurons occurs by expansion or shrinkage in the number of adjacent pre- and postsynaptic appositions within a given multi-synaptic TE. In this manner, the mature CA3 neuron can preserve the physical MF contact which had been established through the normal developmental process of synaptogenesis, while efficiently altering the weighting of the connection over a wide dynamic range (0–40 synaptic equivalents). Indeed, profound increases in the number of discrete synaptic sites with expansion of TEs provides a mechanism for the inactivity-induced increase in mEPSC frequency observed in older hippocampal cultures in this work and previously by others (Burrone et al., 2002; Echegoyen et al., 2007; Han and Stevens, 2009; Murthy et al., 2001; Thiagarajan et al., 2005; Wierenga et al., 2006).

Occasional TEs were observed under normal growth conditions *in vitro* (Figure 4B), suggestive of basal adaptation to local pockets of inactivity that may result from heterogeneity in cell density or innervation in culture (Liu and Tsien, 1995). Thus, the homeostatic conditions we imposed are likely exaggerated versions of naturally occurring and physiologically relevant modes of regulation. The higher incidence of TEs *in vivo* than *in vitro* is consistent with the higher level of spontaneous excitatory activity in cultured neurons relative to the *in vivo* hippocampus, estimated with *ex vivo* recordings (Kim and Tsien, 2008; Echegoyen et al., 2007).

Molecular mechanisms of excrescence formation

How are TEs and the proximal-dendritic homeostatic compartment established? TE formation, like previously reported homeostatic adaptation (Ibata et al., 2008), occurred in response to depletion of intracellular calcium levels, as shown by chelation and store depletion manipulations. Negative regulation of TE expansion is afforded by activity-dependent production of proximally expressed Plk2, which prunes TE size in proportion to the level of overactivity experienced.

Presynaptic synaptoporin was required for functional MF upregulation, and also provides instructive signals necessary for postsynaptic TE formation and/or growth. These data provide a new homeostatic role for synaptoporin, whose precise physiological function has remained unclear. Synaptoporin co-fractionates with synaptic vesicles and is related to synaptophysin, but the expression pattern of synaptoporin is much more restricted to specific subpopulations of neurons (Singec et al., 2002). Future work will be required to determine the downstream synaptoporin signaling cascades that mediate homeostatic regulation.

Interestingly, blockade of GluA1 homomeric AMPARs with philanthotoxin-433 slightly increased mEPSCs amplitudes following inactivity, suggesting that GluA1 homomers are located at relatively weak synapses. The expansion in the number of postsynaptic sites may therefore involve GluA1 homomeric insertion into newly generated PSDs, while existing PSDs are strengthened with GluA1/2 heteromers (Figure 8B). Together, these molecular studies strongly support the idea that giant cluster synapses *in vitro* correspond to MF-TE synapses, and that these unique synapses may therefore mediate HSP *in vivo*.

Excrescences in “circuit-level” homeostatic gain control of mature neurons

Identification of TEs as homeostatic controllers suggests that the locus of HSP is centered on mossy fiber-CA3 synapses in mature hippocampus, which has important implications for the interplay between the highly organized cytoarchitecture of hippocampal circuit elements and the computations they subserve. In this scenario, perforant path input from entorhinal cortex may encode information in distal dendrites of CA3 pyramidal neurons (Figure 8C), while strong, sparse inputs from DG mossy fibers force new information into established CA3 recurrent networks during learning. Indeed, computational studies have suggested that two distinct input systems are essential for the memory-forming and -retrieving functions of the CA3 network (Treves and Rolls, 1992). The strength of MF inputs from DG onto CA3 neurons can be selectively adjusted to reflect the overall network state. Such proximal dendritic gain control of CA3 neuronal input is proposed to “gate” perforant path input to the hippocampus proper, analogous to negative feedback controller elements in circuit design. To help prevent runaway excitation, upregulation of the MF-TE throughput synapse may be balanced by compensatory reduction in recurrent associational-commissural CA3 fibers to help stabilize the intact circuit (Kim and Tsien, 2008; Mitra et al., 2012).

Importantly, this strategy solves the problem of interference of HSP with Hebbian plasticity, as independently tuning proximal CA3 synapses would not interfere with differential synaptic weights established via recurrent associative pathways in the remainder of the CA3 dendritic arbor or elsewhere in the hippocampal network. This model is supported by the observation that infusion of TTX into the adult hippocampus *in vivo* does not alter AMPAR mEPSC amplitude in CA1 pyramidal neurons, but does increase mEPSC frequency (Echegoyen et al., 2007), suggesting that CA1 cells may follow presynaptic adaptation occurring in CA3. Proximal cluster synapses *in vitro*, as well as *in vivo* TEs (Reid et al., 2001), are relatively lacking in NMDARs, further supporting the idea that proximal TEs may be specialized for homeostatic, but not associative plasticity. It is tempting to speculate that a dedicated homeostatic role for MF-CA3 synapses may also explain why the hippocampal CA3 region is particularly susceptible to, and remodeled by, epileptiform activity (Tauck and Nadler, 1985).

In conclusion, we have described a novel conceptual framework of dendritic homeostatic plasticity zones and identified physiological functions for TEs as HSP gain control devices in mature CA3 hippocampal neurons. The ability to generate excrescences *in vitro* should accelerate the molecular dissection of these structures and facilitate elucidation of associated HSP mechanisms.

EXPERIMENTAL PROCEDURES

Cultures, viral infection, and RNAi transfection

Hippocampal cultures prepared from E19 rat embryos were treated at >21 DIV with vehicle control, TTX (1 μM), or PTX (100 μM) for 24 hr. For RNA interference, neurons were transfected at >DIV 21 for 2–3 days prior to treatment with TTX or vehicle control. For viral infection, neurons were transduced between 20–22 DIV for ~18 hr with EGFP, wild-type Plk2, or dominant-negative Plk2 cloned into the pSinRep5 Sindbis virus vector (Invitrogen).

Immunocytochemistry and imaging

Hippocampal cultured neurons were fixed and processed for standard immunocytochemistry. For intensity measurement and spine morphology analysis, images were acquired using an Axiovert 200M (Zeiss) for conventional epifluorescence and Fluoview FV-300 confocal microscope (Olympus), respectively. Confocal z-series image stacks encompassing entire dendrite segments were analyzed using MetaMorph software

(Molecular Devices). Three dimensional reconstructions were created using Neuron Studio (CNIC, Mount Sinai School of Medicine) or Volocity (Improvision) software packages.

Morphological characterization of cell types

CA3 neurons were identified using Py antibody immunocytochemistry (Woodhams et al., 1989). DG neurons were positively immunostained using Prox1 (all DG neurons) and/or CTIP2 (most DG neurons), while CA1 neurons were immunostained using CTIP2 (Williams et al., 2011). Costaining for excitatory synaptic markers Shank or PSD-95 revealed neuronal morphology, allowing for rapid morphological characterization of the 3 principal cell types (see Extended Experimental Methods for description).

Electrophysiology

Neurons were transferred into room temperature extracellular solution containing (in mM): 145 NaCl, 2.5 KCl, 1 $MgCl_2$, 1 $CaCl_2$, 5 HEPES, 5 glucose, and 25 sucrose (330 mOsm, pH 7.4). Whole-cell patch-clamp recordings were made with 3–6 MΩ (Narishige) borosilicate pipettes containing potassium gluconate-based internal solution. Data were collected with an Axiopatch-ID amplifier, Bessel filtered at 2 kHz and digitized at 10 kHz using a Digidata 1440A and Clampex10 software (all from Molecular Devices). Synaptic currents were detected offline using MiniAnalysis (Synaptosoft). For local synaptic stimulation experiments, 2–5 MΩ pipettes were filled with extracellular solution containing 2 mM Ca^{2+} and 500 mM sucrose, and positioned directly above isolated dendrites. Positive pressure released a plume of hyperosmolar solution (visible with DIC optics) (Bekkers and Stevens, 1996; Magee and Cook, 2000). For a subset of experiments, local stimulation was performed in the presence of TTX/BMR with kynurenic acid (200 μM). See Extended Experimental Methods for identification of cell types for recording.

In vivo activity manipulation and quantification of thorny excrescences

Adult mice (C57BL/6, 3-month-old) received a daily intraperitoneal injection for 2 weeks of either PTX (1 mg/kg, i.p.) or diazepam (Dzp, 2 mg/kg, i.p.). All protocols were performed in accordance with the Georgetown University Animal Care and Use Committee. Brain tissues were stained using the FD Rapid Golgi Stain kit (FD Neurotechnologies). Serial brain slices (150 μm) were prepared using a Vibratome (Campden Instruments). Z-series image stacks were used to produce composite images (Adobe Photoshop). Number, size, and total area of dendritic spines were analyzed using MetaMorph software (Molecular Devices).

Statistical analysis

All data represent mean±SEM unless otherwise indicated. For two-sample comparisons vs. controls, unpaired Student's t-test was used. Kolmogorov-Smirnoff (K-S) tests were used for cumulative distributions. For two-sample comparisons within neurons, paired Student's t-tests were used. One-way ANOVA and *post hoc* Tukey tests were used for significance calculations with multiple comparisons.

Detailed methods are available in Extended Experimental Procedures online.

Supplementary Material

Refer to Web version on PubMed Central for supplementary material.

Acknowledgments

KJL, BNQ, AMR, and RB performed experiments. KJL, BNQ, AMR, STL, SV, and DTSP designed and analyzed experiments. KJL, BNQ, SV, and DTSP wrote the manuscript. The authors declare no conflicts of interests. We

thank M. Webb for Py antibodies, and B. Xu and J.Y. Wu for critical comments. This work was supported by NIH/NINDS grants NS048085 and NS075278 (DTSP).

REFERENCES

Amaral D, Dent J. Development of the mossy fibers of the dentate gyrus: A light and electron microscopic study of the mossy fibers and their expansions. J Comp Neurol. 1981; 195:51–86. [PubMed: 7204652]

Bekkers JM, Stevens CF. Cable properties of cultured hippocmpal neurons determined from sucrose-evoked miniature EPSCs. J Neurophysiol. 1996; 75:1250–1255. [PubMed: 8867133]

Burrone J, Byrne MO, Murthy VN. Multiple forms of synaptic plasticity triggered by selective suppression of activity in individual neurons. Nature. 2002; 420:414–418. [PubMed: 12459783]

Carpenter-Hyland EP, Chandler LJ. Homeostatic plasticity during alcohol exposure promotes enlargement of dendritic spines. Eur J Neurosci. 2006; 24:3496–3506. [PubMed: 17229098]

Chicurel M, Harris KM. Three-dimensional analysis of the structure and composition of CA3 branched dendritic spines and their synaptic relationships with mossy fiber boutons in the rat hippocampus. J Comp Neurol. 1992; 325:169–182. [PubMed: 1460112]

Echegoyen J, Neu A, Graber KD, Soltesz I. Homeostatic plasticity studied using in vivo hippocampal activity-blockade: synaptic scaling, intrinsic plasticity and age-dependence. PloS One. 2007; 2:e700. [PubMed: 17684547]

Evers DM, Matta Ja, Hoe H-S, Zarkowsky D, Lee SH, Isaac JTR, Pak DTS. Plk2 attachment to NSF induces homeostatic removal of GluA2 during chronic overexcitation. Nat Neurosci. 2010; 13:1199–1207. [PubMed: 20802490]

Forti L, Bossi M, Bergamaschi A, Villa A, Malgaroli A. Loose-patch recordings of single quanta at individual hippocampal synapses. Nature. 1997; 388:874–878. [PubMed: 9278048]

Galimberti I, Gogolla N, Alberi S, Ferrao Santos A, Muller D, Caroni P. Long-term rearrangements of hippocampal mossy fiber terminal connectivity in the adult regulated by experience. Neuron. 2006; 50:749–763. [PubMed: 16731513]

Goel A, Lee H-K. Persistence of experience-induced homeostatic synaptic plasticity through adulthood in superficial layers of mouse visual cortex. J Neurosci. 2007; 27:6692–6700. [PubMed: 17581956]

Han EB, Stevens CF. Development regulates a switch between post- and presynaptic strengthening in response to activity deprivation. Proc Nat Acad Sci. 2009; 106:10817–10822. [PubMed: 19509338]

Hatanaka Y, Mukai H, Mitsuhashi K, Hojo Y, Murakami G, Komatsuzaki Y, Sato R, Kawato S. Androgen rapidly increases dendritic thorns of CA3 neurons in male rat hippocampus. Biochem Biophys Res Commun. 2009; 381:728–732. [PubMed: 19254689]

Henze DA, Card JP, Barrionuevo G, Ben-ari Y, Lauri SE, Segerstråle M, Vesikansa A, Maingret F, Mulle C, Collingridge L, et al. Large Amplitude Miniature Excitatory Postsynaptic Currents in Hippocampal CA3 Pyramidal Neurons Are of Mossy Fiber Origin. J Neurophysiol. 1997; 77:1075–1086. [PubMed: 9084583]

Ibata K, Sun Q, Turrigiano GG. Rapid synaptic scaling induced by changes in postsynaptic firing. Neuron. 2008; 57:819–826. [PubMed: 18367083]

Jonas P, Major G, Sakmann B. Quantal components of unitary EPSCs at the mossy fiber synapse on CA3 pyramidal cells of rat hippocampus. J Physiol. 1993; 472:615–663. [PubMed: 7908327]

Kim J, Tsien RW. Synapse-specific adaptations to inactivity in hippocampal circuits achieve homeostatic gain control while dampening network reverberation. Neuron. 2008; 58:925–937. [PubMed: 18579082]

Kolomeets NS, Orlovskaya DD, Uranova NA. Decreased numerical density of CA3 hippocampal mossy fiber synapses in schizophrenia. Synapse. 2007; 61:615–621. [PubMed: 17476682]

Lee KJ, Lee Y, Rozeboom A, Lee J-Y, Udagawa N, Hoe H-S, Pak DTS. Requirement for Plk2 in orchestrated ras and rap signaling, homeostatic structural plasticity, and memory. Neuron. 2011; 69:957–973. [PubMed: 21382555]

Liu G, Tsien RW. Properties of synaptic transmission at single hippocampal synaptic boutons. Nature. 1995; 375:404–408. [PubMed: 7760934]

Magee JC, Cook EP. Somatic EPSP amplitude is independent of synapse location in hippocampal pyramidal neurons. Nat Neurosci. 2000; 3:895–903. [PubMed: 10966620]

Malinow R, Malenka RC. AMPA receptor trafficking and synaptic plasticity. Ann Rev Neurosci. 2002; 25:103–126. [PubMed: 12052905]

Mellor J, Nicoll Ra. Hippocampal mossy fiber LTP is independent of postsynaptic calcium. Nat Neurosci. 2001; 4:125–126. [PubMed: 11175870]

Mitra A, Mitra SS, Tsien RW. Heterogeneous reallocation of presynaptic efficacy in recurrent excitatory circuits adapting to inactivity. Nat Neurosci. 2012; 15:250–257. [PubMed: 22179109]

Murthy VN, Schikorski T, Stevens CF, Zhu Y. Inactivity produces increases in neurotransmitter release and synapse size. Neuron. 2001; 32:673–682. [PubMed: 11719207]

O'Brien RJ, Kamboj S, Ehlers MD, Rosen KR, Fischbach GD, Huganir RL. Activity-dependent modulation of synaptic AMPA receptor accumulation. Neuron. 1998; 21:1067–1078. [PubMed: 9856462]

Pak DTS, Sheng M. Targeted protein degradation and synapse remodeling by an inducible protein kinase. Science. 2003; 302:1368–1373. [PubMed: 14576440]

Pozo K, Goda Y. Unraveling mechanisms of homeostatic synaptic plasticity. Neuron. 2010; 66:337–351. [PubMed: 20471348]

Ramon y Cajal, S. Histologie du Systeme Nerveux de l'homme et des Vertebres. Paris: Maloine; 1911.

Reid CA, Fabian-Fine R, Fine A. Postsynaptic calcium transients evoked by activation of individual hippocampal mossy fiber synapses. J Neurosci. 2001; 21:2206–2214. [PubMed: 11264296]

Reyes M, Stanton PK. Induction of hippocampal long-term depression requires release of Ca2+ from separate presynaptic and postsynaptic intracellular stores. J Neurosci. 1996; 16:5951–5960. [PubMed: 8815877]

Seeburg DP, Feliu-Mojer M, Gaiottino J, Pak DTS, Sheng M. Critical role of CDK5 and Polo-like kinase 2 in homeostatic synaptic plasticity during elevated activity. Neuron. 2008; 58:571–583. [PubMed: 18498738]

Singec I, Knoth R, Ditter M, Hagemeyer C, Rosenbrock H, Frotscher M, Volk B. Synaptic vesicle protein synaptoporin is differently expressed by subpopulations of mouse hippocampal neurons. J Comp Neurol. 2002; 452:139–152. [PubMed: 12271488]

Stewart MG, Davis HA, Sandi C, Kraev IV, Rogachevsky W, Peddie CJ, Rodriguez JJ, Cordero MI, Donohue HS, Gabbott PL, et al. Stress suppresses and learning induces plasticity in CA3 of rat hippocampus: a three-dimensional ultrastructural study of thorny excrescences and their postsynaptic densities. Neuroscience. 2005; 131:43–54. [PubMed: 15680690]

Takai Y. Nectin and afadin: novel organizers of intercellular junctions. J Cell Sci. 2003; 116:17–27. [PubMed: 12456712]

Tauck DL, Nadler JV. Evidence of functional mossy fiber sprouting in hippocampal formation of kainic acid-treated rats. J Neurosci. 1985; 5:1016–1022. [PubMed: 3981241]

Thiagarajan TC, Lindskog M, Tsien RW. Adaptation to synaptic inactivity in hippocampal neurons. Neuron. 2005; 47:725–737. [PubMed: 16129401]

Treves A, Rolls ET. Computational constraints suggest the need for two distinct input systems to the hippocampal CA3 network. Hippocampus. 1992; 2:189–199. [PubMed: 1308182]

Tsamis IK, Mytilinaios GD, Njau NS, Fotiou FD, Glaftsi S, Costa V, Baloyannis JS. Properties of CA3 dendritic excrescences in Alzheimer's disease. Curr Alzheimer Res. 2010; 7:84–90. [PubMed: 20205674]

Turrigiano GG. The self-tuning neuron: synaptic scaling of excitatory synapses. Cell. 2008; 135:422–435. [PubMed: 18984155]

Turrigiano GG, Leslie KR, Desai NS, Rutherford LC, Nelson SB. Activity-dependent scaling of quantal amplitude in neocortical neurons. Nature. 1998; 391:892–896. [PubMed: 9495341]

Turrigiano GG, Nelson SB. Hebb and homeostasis in neuronal plasticity. Curr Opin Neurobiol. 2000; 10:358–364. [PubMed: 10851171]

Wierenga CJ, Ibata K, Turrigiano GG. Postsynaptic expression of homeostatic plasticity at neocortical synapses. J Neurosci. 2005; 25:2895–2905. [PubMed: 15772349]

Wierenga CJ, Walsh MF, Turrigiano GG. Temporal regulation of the expression locus of homeostatic plasticity. J Neurophysiol. 2006; 96:2127–2133. [PubMed: 16760351]

Williams ME, Wilke SA, Daggett A, Davis E, Otto S, Ravi D, Ripley B, Bushong EA, Ellisman MH, Klein G, et al. Cadherin-9 regulates synapse-specific differentiation in the developing hippocampus. Neuron. 2011; 71:640–655. [PubMed: 21867881]

Woodhams PL, Webb M, Atkinson DJ, Seeleyl PJ. A monoclonal antibody, Py, distinguishes different classes of hippocampal neurons. J Neurosci. 1989; 9:2170–2181. [PubMed: 2470877]

HIGHLIGHTS

- Mature hippocampal neurons have spatially segregated homeostatic plasticity *in vitro*.
- Adaptation modulates mossy fiber synapses onto CA3 neuron thorny excrescences (TEs).
- Mossy fiber synaptoporin is necessary and sufficient for homeostatic plasticity.
- Network activity and Plk2 selectively regulate TE structural plasticity *in vivo*.

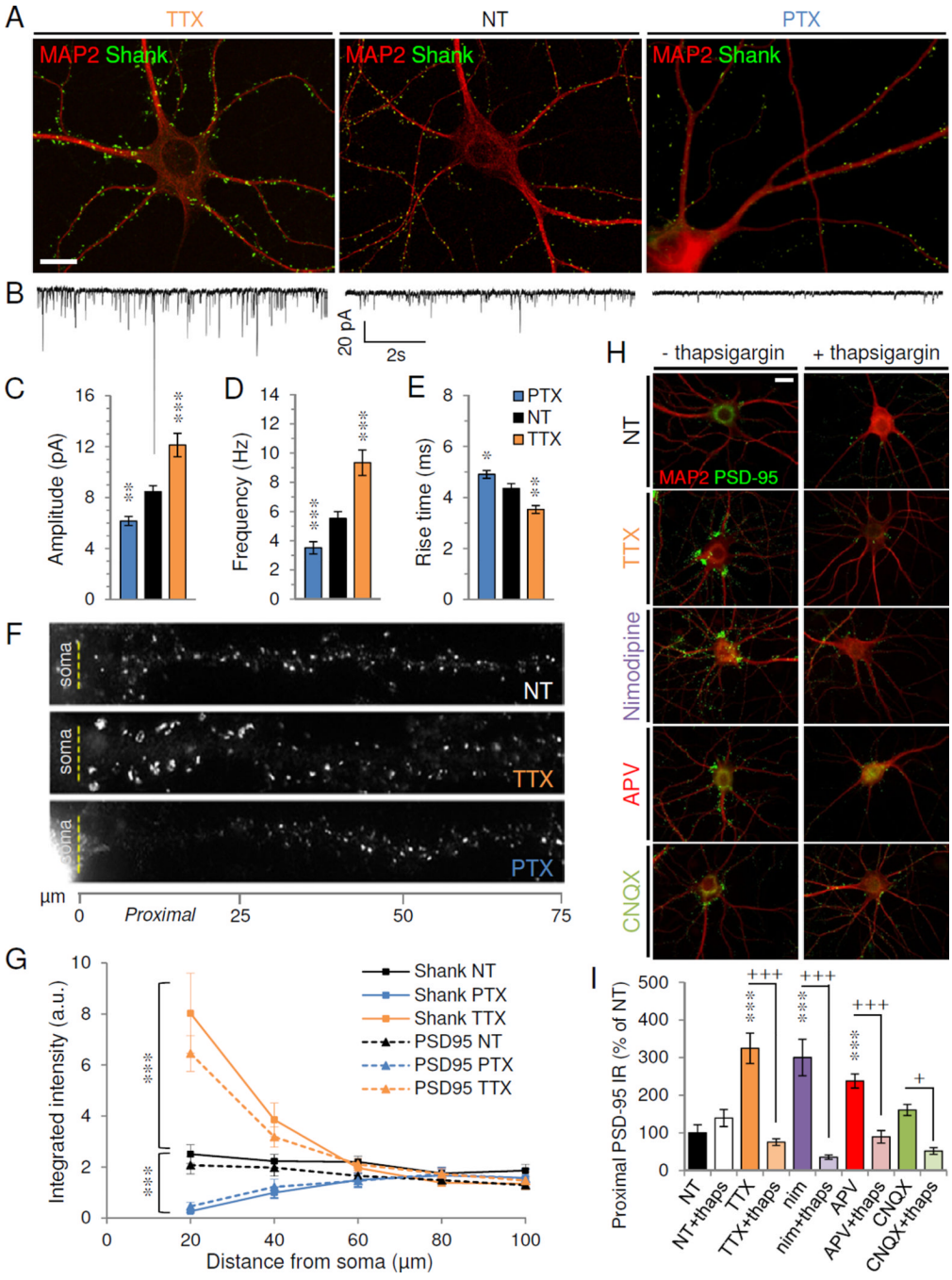

Figure 1. Homeostatic changes are confined to proximal dendrites

(**A–B**) Cultured hippocampal neurons were treated at DIV 21 with TTX (left), vehicle (nontreated, NT) (center) or PTX (right) before immunostaining (**A**) or whole-cell recording (**B**). (**A**) Immunostaining for excitatory synaptic marker Shank (green) and dendritic marker MAP2 (red). (**B**) Representative 10s voltage-clamp traces of AMPAR-mediated mEPSCs. (**C–E**) Average mEPSC amplitude (**C**), frequency (**D**), and rise time (**E**) from neurons with indicated treatments (n=21–29 cells/group). **P*<0.05, ***P*<0.01, ****P*<0.001 vs. NT. (**F**) Shank staining in dendrites straightened to show distance from soma (dashed line). (**G**) Integrated intensity of Shank (solid lines) or PSD-95 (dotted) staining with distance from

soma. ***P<0.0001 vs. NT (n=12 cells/group). (**H**) PSD-95 (green) and MAP2 (red) staining of neurons treated for 24 hrs with vehicle (NT), TTX, Nimodipine (nim), APV, or CNQX in the absence (left) or presence (right) of thapsigargin (thaps). (**I**) PSD-95 immunoreactivity in proximal dendrites (<20μm) of neurons (n=10) in conditions indicated, normalized to NT. ***P<0.001 vs. NT; +P<0.05, +++P<0.001 vs. thapsigargin. All scale bars, 20 μm. Data are means±SEM. See also Figure S1.

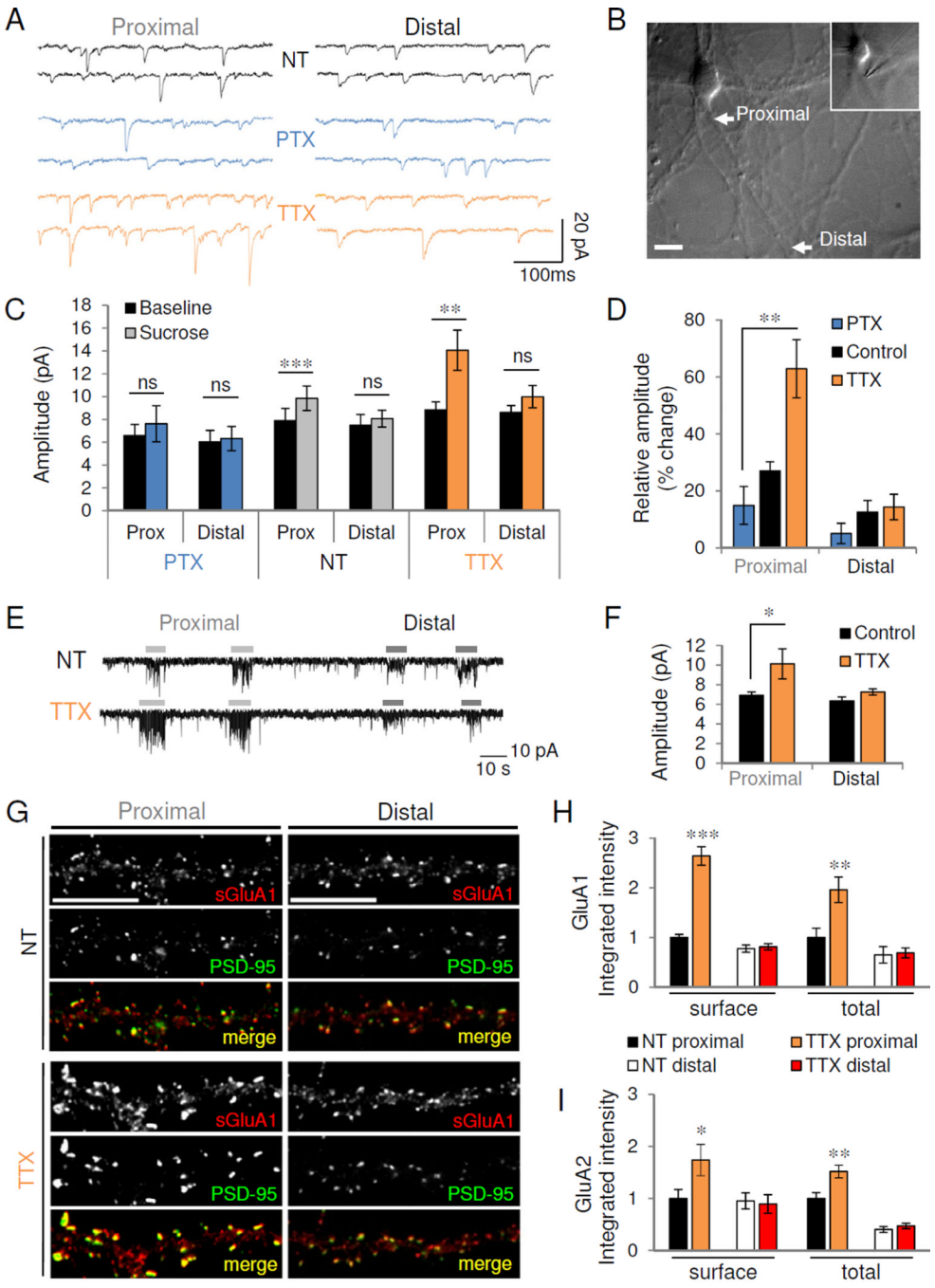

Figure 2. HSP selectively regulates proximal synaptic efficacy and AMPAR accumulation

(**A**) Representative 500ms traces of mEPSCs recorded during proximal (left) and distal (right) stimulation of control (NT) or activity-modulated neurons. (**B**) DIC image of neuron stimulated focally at proximal (~15 μm from soma, see inset) and distal (~120 μm) dendritic locations. Scale, 20 μm. (**C**) Average mEPSC amplitude recorded before (baseline) or after (sucrose) stimulation of proximal and distal synapses for conditions indicated (n=11 NT neurons, 12 TTX, 5 PTX); ns, not significant; ** P=0.0048, *** P=5.91×10^{-6}. (**D**) Percent change in mEPSC amplitude over baseline during proximal and distal stimulation. ** P=0.009. (**E**) Miniature EPSCs recorded from a control (top) and TTX-treated (bottom)

neuron during kynurenic acid blockade. Bars indicate sucrose stimulation of proximal and distal dendrites. (**F**) Mean mEPSC amplitude evoked during kynurenic acid blockade (n=4 NT, 5 TTX). **P*=0.027. (**G**) Immunostaining for surface GluA1 (sGluA1, red) and PSD-95 (green) in proximal (left) and distal (right) dendrites of control (NT) or TTX-treated neurons. Scale, 10 μm. (**H–I**) Quantification of normalized GluA1 (**H**) and GluA2 (**I**) immunoreactivity in proximal and distal dendrites (n=11–13). **P*<0.05, ***P*<0.01, ****P*<0.001. For distal dendrites, t-test vs. NT: surface GluA1, *P*=0.71; total GluA1, *P*=0.83; surface GluA2, *P*=0.81; total GluA2, *P*=0.38. Data are means±SEM. See also Figure S2.

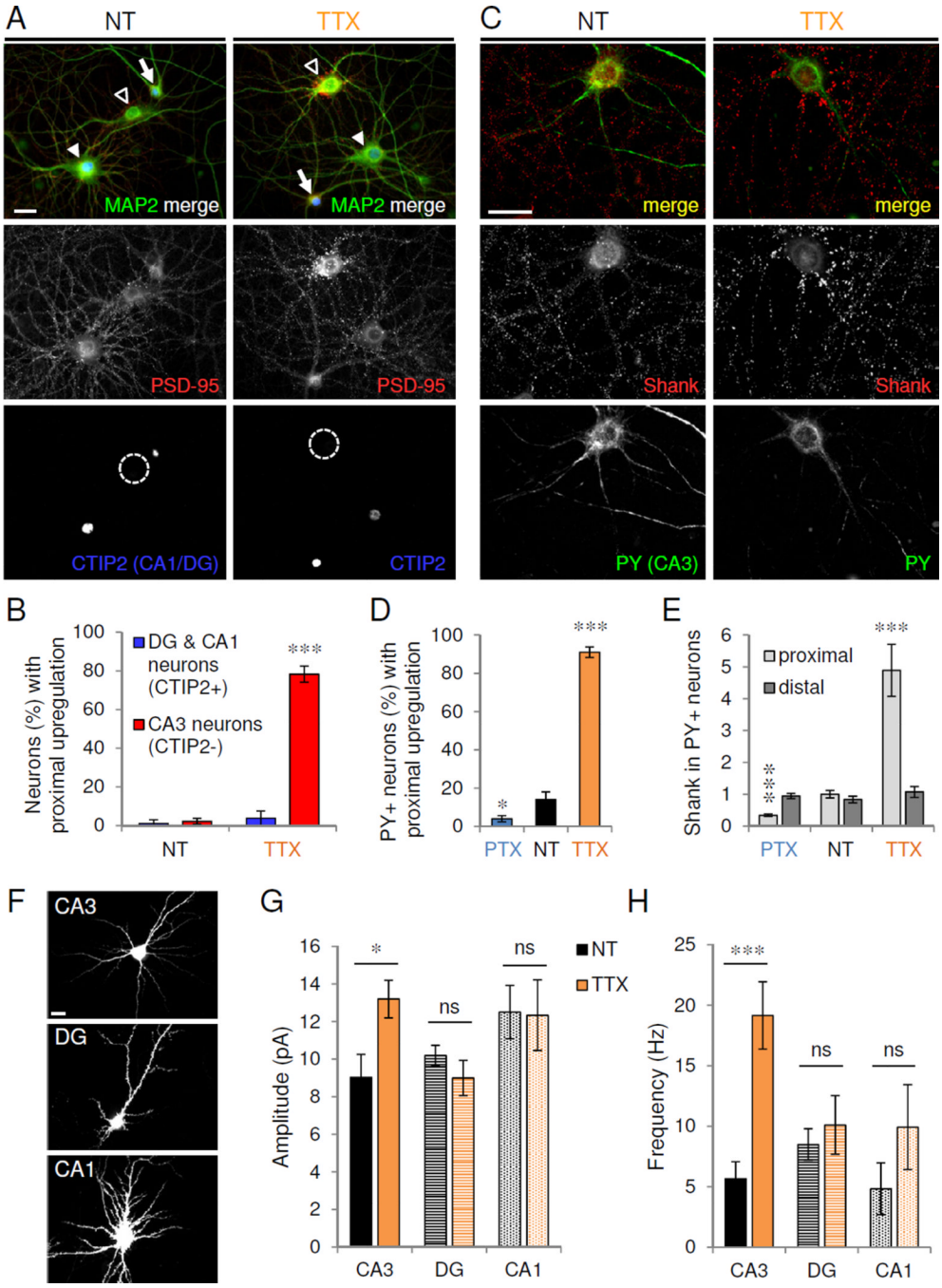

Figure 3. Proximal HSP occurs preferentially in CA3 neurons

(**A**) Cultured hippocampal neurons (>DIV 21) treated with vehicle (NT) or TTX and immunostained for MAP2 (green), PSD-95 (red) and CA1/DG-specific marker CTIP2 (blue; dotted circle indicates CTIP2-negative neuron). Open arrowhead, CA3; filled arrowhead, CA1; arrow, DG. (**B**) Proportion of CTIP2-positive and -negative neurons with proximal PSD-95 upregulation under activity conditions indicated. ***P=7.71×10^{-6}, n=4 independent experiments of 100–150 neurons/treatment. (**C**) Neurons immunostained for excitatory synaptic marker Shank (red) and CA3 pyramidal neuron marker Py (green) in control (NT) and TTX conditions. (**D**) Proportion of Py+ CA3 neurons with proximal upregulation under

activity conditions indicated (n=100 from 10 independent experiments). *$P<0.05$, ***$P<0.001$. (**E**) Shank immunoreactivity in proximal and distal dendrites from control and activity-modulated CA3 neurons (n=10). ***$P<0.001$. (**F**) GFP-transfected CA3, DG, and CA1 neurons visualized at time of recording. (**G–H**) Average mEPSC amplitude (**G**) and frequency (**H**) recorded from GFP-expressing CA3, DG, or CA1 cells (n=5–15) under conditions indicated; ns, $P>0.26$; *$P=0.016$, ***$P=2.3\times10^{-4}$. Scale bars, 20 μm. Data are means±SEM. See also Figure S3.

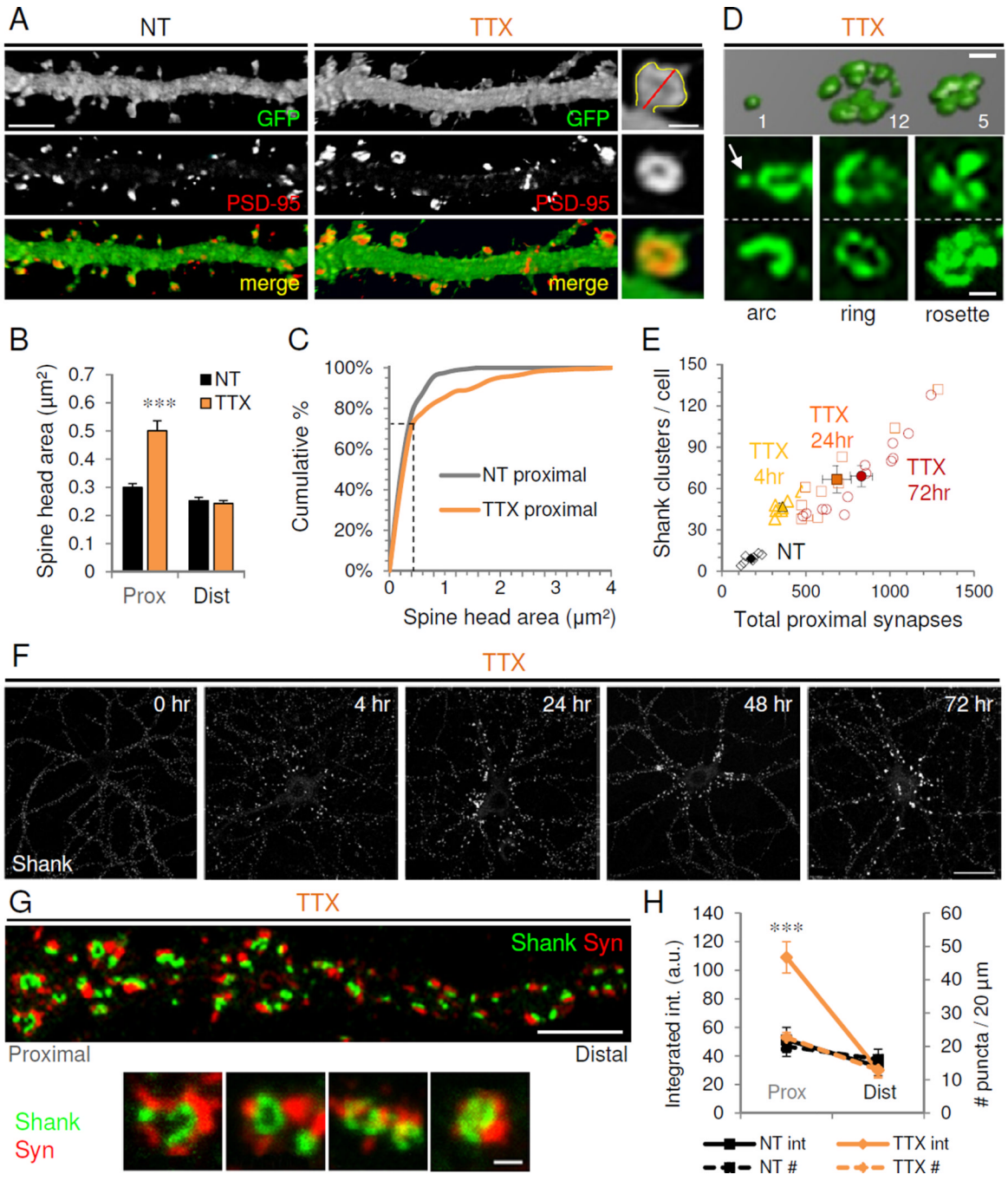

Figure 4. Inactivity induces proximal giant cluster synapses

(**A**) Confocal images of proximal dendrites from GFP-expressing nontreated (NT) and TTX-treated cultured hippocampal neurons (21 DIV) immunostained against GFP fill (green) and PSD-95 (red). Right, higher magnification view of a giant spine showing method for quantifying spine head area (yellow line) and spine length (red). Scales, 5 µm for dendrites, 1 µm for inset. (**B**) Average spine head area in proximal and distal dendrites of control (NT) and TTX-treated neurons. ***P<0.001 (n=8). Data are means±SEM. **(C)** Cumulative distribution of spine head areas in proximal dendrites of control and TTX-treated neurons; ***P<0.005, K-S test (NT=322 vs. TTX=337 spines). Note the non-multiplicative shift

occurring preferentially in the larger spine population (indicated with dotted lines). (**D**) 3D confocal microscopy reconstruction of Shank immunostaining from a TTX-treated neuron showing a simple synapse (left) and neighboring giant cluster synapses. Values indicate number of PSD lobes per cluster (see **Methods** for calculation). Below, common arrangements of clusters (arrow indicates simple synapse). Scale, 1 μm. (**E**) Correlation between total number of excitatory synapses in proximal dendrites and number of clusters for control (NT) and TTX-treated neurons at 4, 24, and 72 hr. Open symbols, individual neurons; filled symbols, mean population values±SEM. (**F**) Timecourse of Shank immunostaining in TTX-treated neurons. Scale, 20 μm. (**G**) TTX-treated neuron immunostained for presynaptic synaptophysin (Syn, red) and postsynaptic Shank (green). Scale, 5 μm. Below, high magnification views of Shank and Syn giant clusters. Scale, 1 μm. (**H**) Syn integrated intensity (solid lines) and number of Syn puncta (dotted lines) in proximal and distal dendrites of NT or TTX neurons; ***$P<0.001$, t-test vs. NT. See also Figure S4.

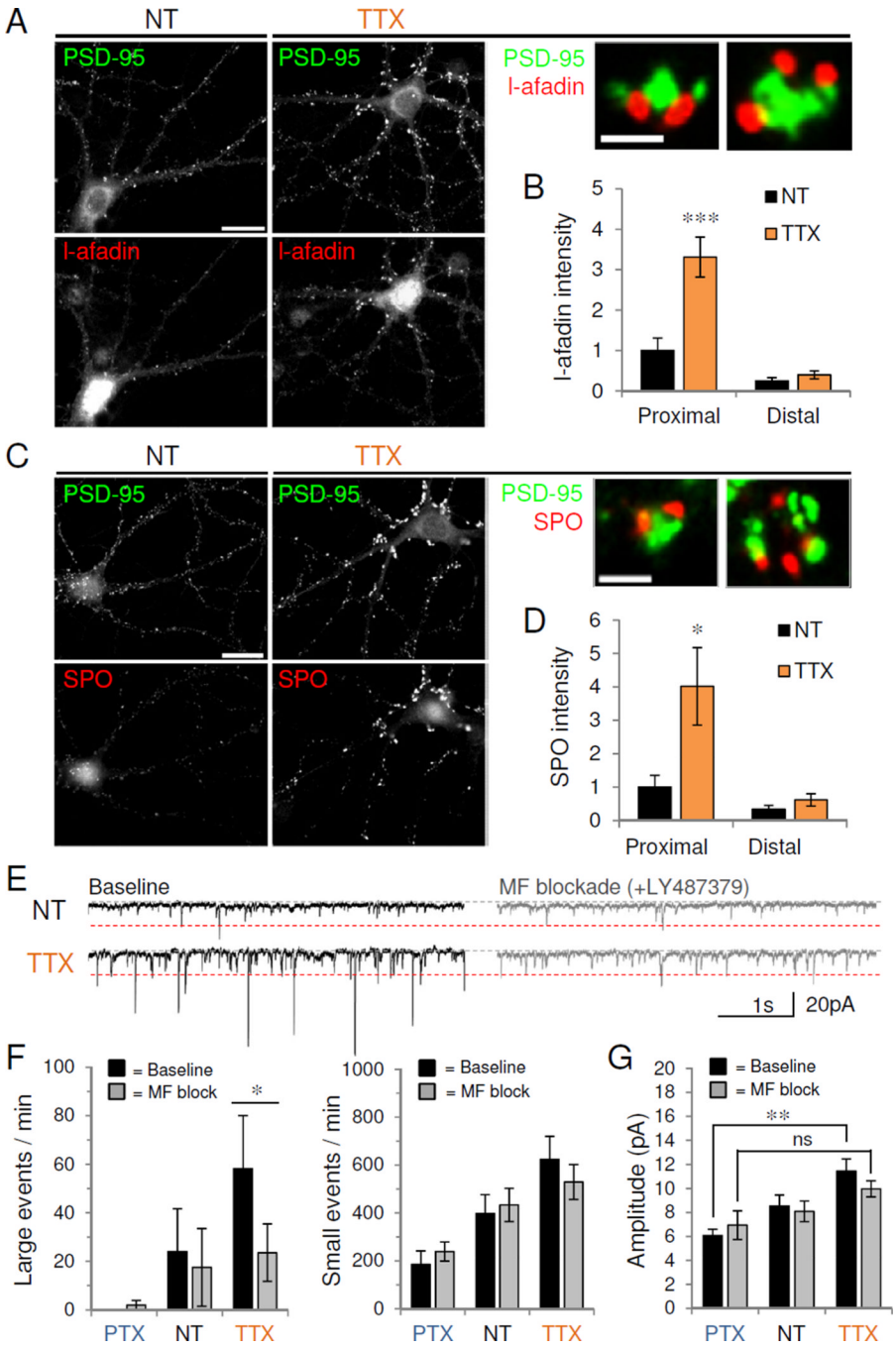

Figure 5. Inactivity promotes mossy fiber-TE synapse upregulation

(**A,C**) Control (NT) or TTX-treated CA3 neurons (DIV 24) stained for endogenous PSD-95 (green) with either (**A**) TE puncta adherentia protein, l-afadin (red) or (**C**) presynaptic mossy fiber protein, synaptoporin (SPO, red). Scale, 20 μm. High magnification views show two representative proximal cluster synapses with merged co-staining. Scale, 1 μm. (**B,D**) Quantification of immunoreactivity for (**B**) l-afadin or (**D**) SPO in control or TTX-treated proximal and distal dendrites (n=10–11). **P*<0.05, ****P*<0.001. (**E**) Representative 5s voltage-clamp traces of mEPSCs recorded from control (NT) or TTX-treated neurons before (left) and after (right) acute mossy fiber blockade with LY487379. Red dotted line, 20 pA

cutoff for small vs. large events. (**F**) Average number of large (>20 pA, left) and small amplitude (<20 pA, right) events per minute recorded from control or activity-modulated neurons before and after LY487379 (n=8). **P*=0.032. (**G**) Average mEPSC amplitude before and after LY487379 application; ns, *P*=0.08; ***P*<0.01 (n=5–9). Data are means±SD. See also Figure S5.

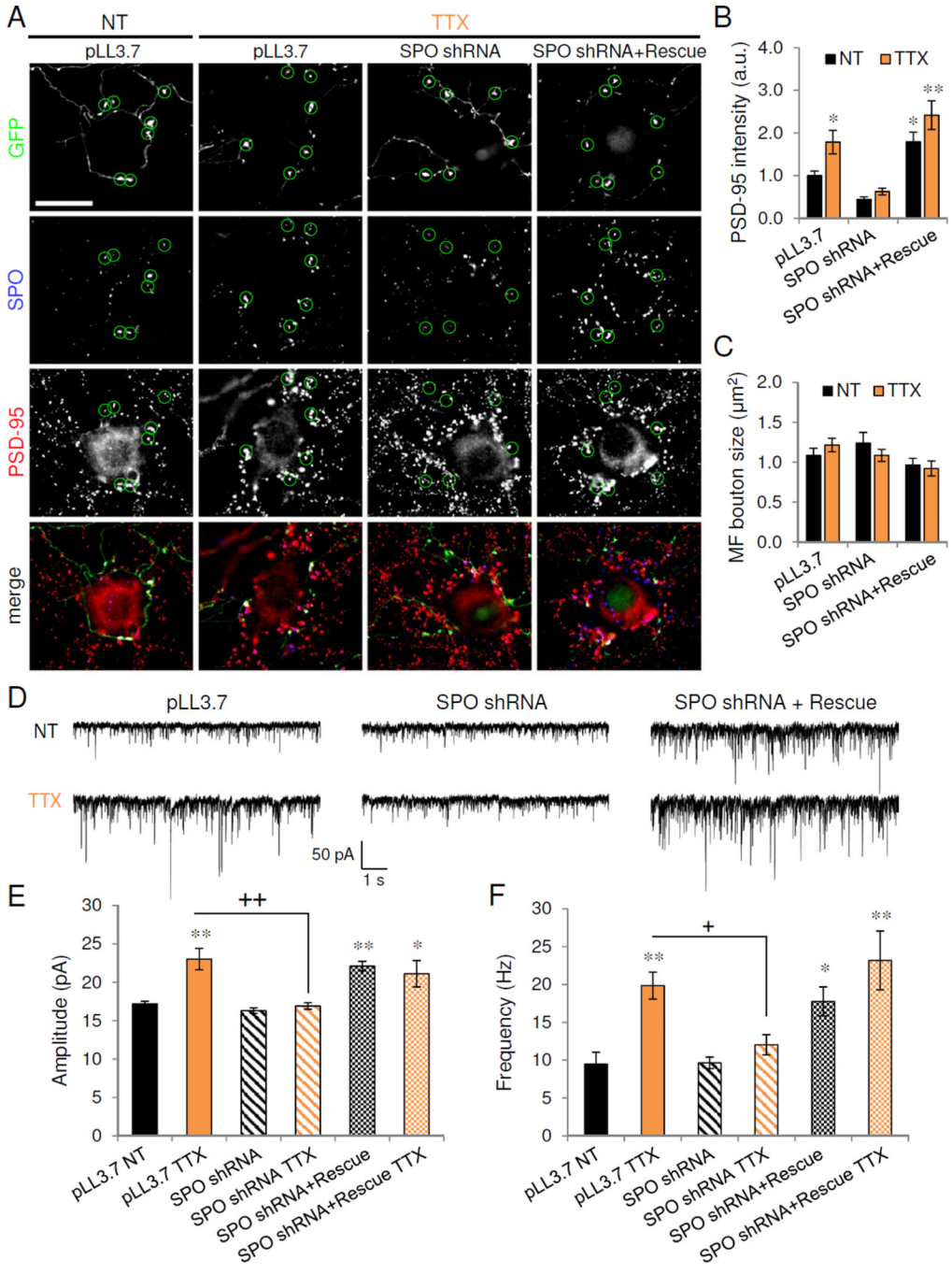

Figure 6. Presynaptic synaptoporin is required for homeostatic adaptation to inactivity

(**A**) PSD-95 (red) immunolabeling of untransfected CA3 neurons receiving presynaptic innervation from synaptoporin (SPO)-positive mossy fiber terminals originating from GFP-expressing dentate granule (DG) cells transfected with vector control (pLL3.7), SPO shRNA, or SPO shRNA and SPO rescue construct. Circles indicate large GFP-positive presynaptic mossy fiber boutons. Scale, 20 μm. (**B**) Normalized PSD-95 puncta intensity in CA3 neurons opposing GFP-positive mossy fiber boutons transfected with vector control, SPO shRNA, or SPO shRNA+rescue construct, and treated as shown; n=12, * $P<0.05$, ** $P<0.01$. (**C**) Mossy fiber bouton size from GFP-positive DG neurons transfected with

constructs and treated as indicated. (**D**) Representative 10s voltage-clamp trace of AMPAR-mEPSCs recorded from untransfected targets of GFP-positive mossy fibers. DG cells were transfected with constructs indicated prior to treatment with vehicle (NT) or TTX. (**E–F)** Average amplitude (**E**) and frequency (**F**) of AMPAR-mEPSCs recording from untransfected control (NT) and TTX cells receiving presynaptic innervation from GFP-positive mossy fibers of DG cells transfected with constructs indicated. **P*<0.05, ***P*<0.01 vs. NT; ns = *P*>0.05, + *P*<0.05, ++ *P*<0.01 vs. TTX (n=6–11). Data are means±SEM. See also Figure S6.

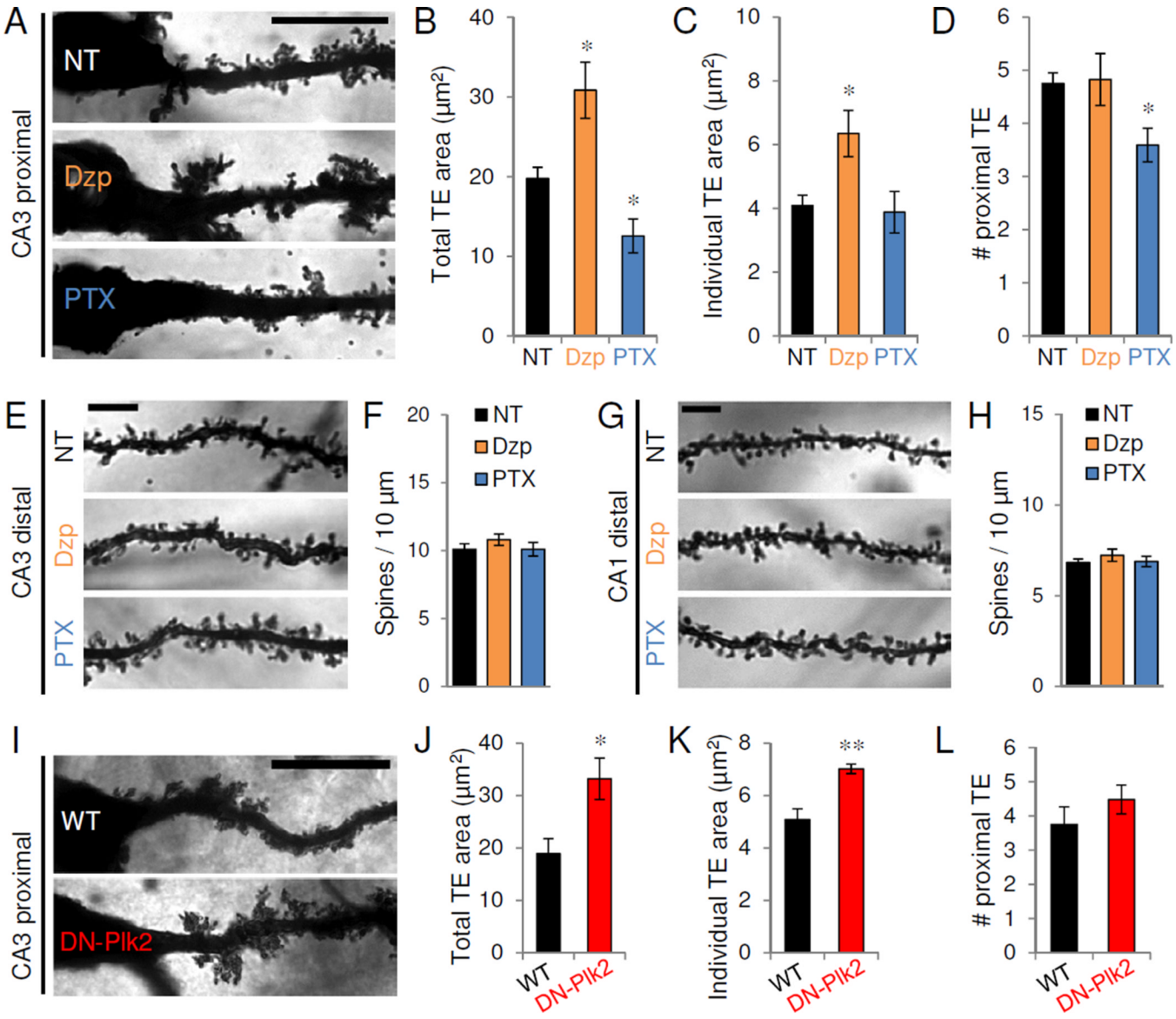

Figure 7. Network activity and Plk2 regulate TEs *in vivo*

(**A**) Golgi staining of representative proximal apical dendrites of CA3 pyramidal neurons in 3-month-old mice after chronic (14 d) injection of vehicle control (NT), diazepam (Dzp), or PTX (n=5–6 mice/condition). Scale, 20 µm. (**B–D**) Quantification of total TE area (**B**), individual TE area (**C**), and average number of TE (**D**) within proximal (<30 µm from soma) apical CA3 dendrites (n=17–20 neurons from 5–6 mice/condition). **P*<0.05. (**E,G**) Golgi staining of representative distal apical dendrites of CA3 (**E**) or CA1 (**G**) pyramidal neurons in 3-month-old mice after chronic (14 d) injection of vehicle control (NT), diazepam (Dzp), or PTX. Scale bars, 5 µm. (**F,H**) Average distal dendritic spine density (#/10 µm) from CA3 (**F**) and CA1 (**H**) neurons. Data expressed as average±SE of animal means (n=5–6 mice/condition; 2–3 neurons/animal). (**I**) Representative proximal apical CA3 dendrites from control wild-type (WT) mice and dominant negative-Plk2 (DN-Plk2) transgenic littermates. (**J–L**) Total TE area (**J**), individual TE area (**K**), and average number of TE (**L**) within proximal (<30 µm) apical dendrites (n=12–13 neurons from 5 mice/genotype). **P*<0.05, ***P*<0.01. Scale, 20 µm. Data are means±SEM. See also Figure S7.

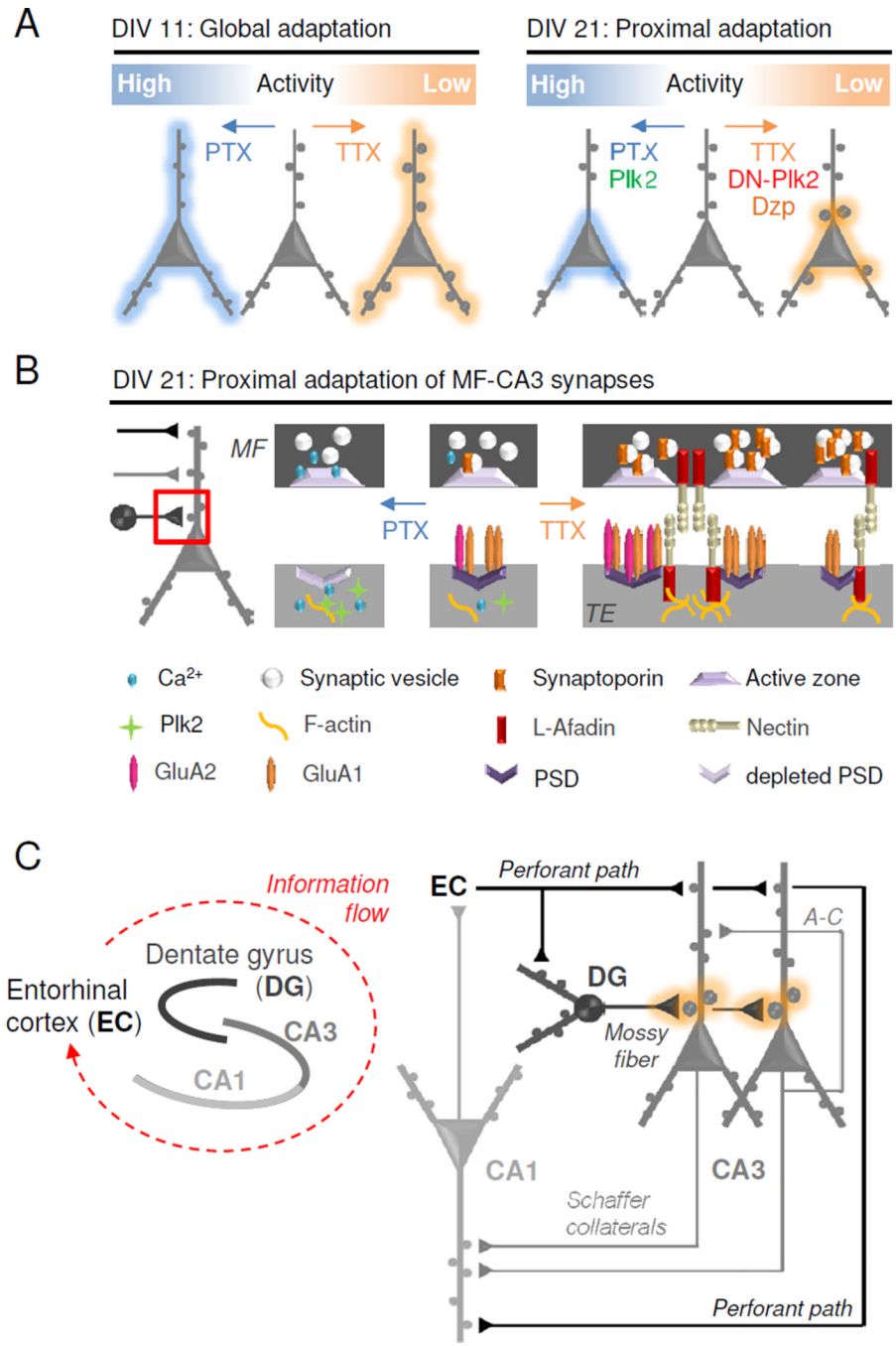

Figure 8. Proposed homeostatic gain control locus at mossy fiber-CA3 synapses

(**A**) Schematic diagram of homeostatic regulation in developing (DIV 11, left) and mature (DIV 21, right) hippocampal neurons. (**B**) Model showing molecular mechanisms of selective synaptic adaptation between mossy fibers (MF) and TEs in mature neurons. Hyperactivity (PTX): Presynaptic Ca^{2+} influx leads to diminished MF expression of synaptoporin (SPO) and less vesicular release. Postsynaptic Ca^{2+} influx induces Plk2 expression, depletion of PSD components, and synaptic loss. Inactivity (TTX): Decreased presynaptic Ca^{2+} influx increases SPO expression and vesicular release in mossy fibers. Diminished postsynaptic Ca^{2+} influx induces l-afadin expression and burgeoning of PSDs,

increasing the number of synaptic sites. GluA1 homomers may be incorporated into nascent synapses while existing synapses are strengthened by GluA1/2 heteromers. (**C**) Simplified hippocampal circuit diagram with MF-TE gain control (orange). Information enters the hippocampus from the entorhinal cortex (EC) via the perforant path (PP) which innervates dentate granule (DG) cells as well as distal CA3 and CA1 dendrites. Hebbian plasticity may occur in distal dendrites receiving recurrent (associational-commissural (A–C) CA3-CA3) and throughput (PP-CA3/CA1 and CA3-CA1) innervation. Homeostatic plasticity occurs at the proximal synapses of CA3 neurons which receive mossy fiber input from DG neurons.